Contribution from the Departments of Chemistry, Columbia University, New York, New York 10027, and Washington University, St. Louis, Missouri 63130

Synthesis, Characterization, and Solution Chemistry of a Family of Protein-Binding Inorganic Complexes: Bis(imidazole)(amino acid-*N*,*N*-diacetato)chromium(III)

Jeffrey R. Bocarsly,[†,‡] Michael Y. Chiang,[§] Leshauna Bryant,[†] and Jacqueline K. Barton*[,†,∥]

Received May 8, 1990

The synthesis and characterization of a family of transition-metal complexes containing amino acid substituents, which has shown an array of recognition characteristics relevant to association with proteins, is described. These molecules are based upon the bis(imidazole)(nitrilotriacetato)chromium(III) core, with the series generated through substitutions of amino acid side chains onto the methylene position of one of the chelate rings. The synthesis of the series has been achieved through the intermediate bis(aquo)(nitrilotriacetato)chromium(III) (**1**), previously not isolated, and by the use of substituted analogues. The solvated, solid-state structures of two members of the family, bis(imidazole)(*l*-leucine-*N*,*N*-diacetato)chromium(III) (**3a**) and bis(imidazole)(*l*-phenylalanine-*N*,*N*-diacetato)chromium(III) (**4a**) have been established by single-crystal X-ray diffraction studies. Crystal data: (**3a**, orthorhombic, space group $P2_12_12_1$, a = 8.576 (3) Å, b = 15.784 (9) Å, c = 15.648 (6) Å, V = 2118 (2) Å^3, Z = 4, $R(F_o)$ = 0.0421 ($R_w(F_o)$ = 0.0627); **4a**, orthorhombic, space group $P2_12_12_1$, a = 9.601 (4) Å, b = 14.045 (4) Å, c = 37.235 (11) Å, V = 5021 (3) Å^3, Z = 8, $R(F_o)$ = 0.0846 ($R_w(F_o)$ = 0.0985). The solid-state intermolecular interactions of these complexes are relevant to protein binding and include not only hydrogen-bonding interactions but also aromatic-aromatic interactions (in **4a**). Electronic and circular dichroic parameters for the complexes are reported, and the stereochemical course of the aquation of the parent bis(imidazole)(nitrilotriacetato)chromium(III) (**2**) in solution is described. When ^{2}H NMR methods are used on the deuterated analogue, the imidazole cis to three carboxylates is found to be the leaving group.

Introduction

Work in this laboratory has focused on the design and synthesis of transition-metal complexes that can interact with biopolymers through an ensemble of weak noncovalent interactions based upon shape selection[1] in a geometry-specific fashion. While recent attention has centered primarily on nucleic acids, we have been concerned also with developing probes for protein structures. This effort may be considered as the first step toward the rational design of both inorganic pharmaceuticals as well as site-specific inorganic labels for protein structures. Transition-metal complexes offer the advantages of well-defined coordination geometries, multiple interchangeable biologically relevant ligand sets, a breadth of informative spectroscopic characteristics, and a potentially rich solution chemistry at the metal center. We have recently described how the magnetic characteristics of such complexes may be used to probe their binding location and mode on a protein surface, using the method of nuclear Overhauser effect quenching, and how manipulation of recognition elements in the ligand set can lead to interesting perturbations in the binding characteristics.[2] In this report, we describe the synthesis and characterization of the family (Chart I) of complexes designed for this work; in addition, we explore biologically relevant interactions observed in the solid-state structures and relevant solution-state chemistry of these complexes.

This family of complexes is based on the nitrilotriacetate ligand, which is a member of the extensive family of complexon ligands.[3] The ligand can be derivatized to contain a pendant amino acid side chain by a simple condensation of the desired amino acid with 2 equiv of haloacetic acid. By use of this method, several derivatized chromium(III)-nitrilotriacetate moieties have been synthesized earlier;[4] however, none have been characterized structurally. The chromium-nitrilotriacetate system appeared to be a promising choice as a starting point in this work, due to the known stability of the system,[4] the relative ease with which the ligand may be derivatized with biologically relevant moieties, the availability of the two remaining cis coordination sites for chemistry at the metal center, and the magnetic characteristics of the chromium(III) ion.

Experimental Section

Physical Measurements.[5] Chemical ionization mass spectra were recorded on a Ribermag R10-10 mass spectrometer using either NH_3 or CH_3 as reagent gas. FAB mass spectra were recorded on a JEOL mass spectrometer using a matrix of 3-nitrobenzyl alcohol in a beam of 7-KeV accelerated Xe atoms. Infrared spectra were recorded on a Perkin-Elmer 1600 FTIR instrument in ratio mode. The samples were prepared as KBr pellets. A total of 8-16 scans were collected per spectrum.

Visible spectra were recorded on a Cary-219 or a Varian DMS-300 UV-visible spectrophotometer. The solution concentrations were determined by weighing for all methanol solutions and for aqueous solutions of $Cr(NTA)(H_2O)_2$ (**1**). The imidazole-containing complexes dissolve slowly in water where the thermal reaction is appreciable; therefore,

Chart I

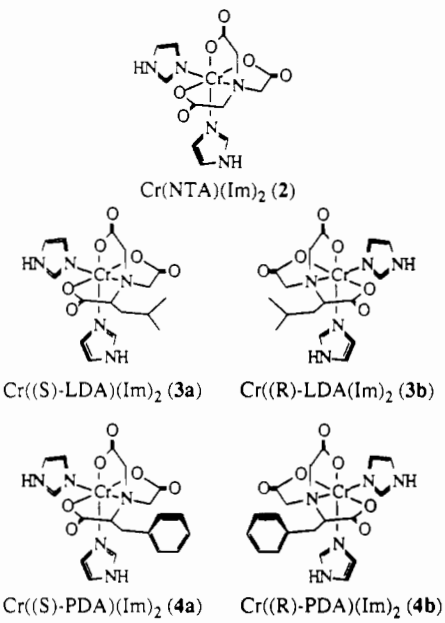

* To whom correspondence should be addressed.
† Columbia University.
‡ Present address: Department of Chemistry, Yale University, New Haven, CT 06511.
§ Washington University.
∥ Present address: Division of Chemistry and Chemical Engineering, California Institute of Technology, Pasadena, CA 91125.

(1) Barton, J. K. *Science* **1986**, *233*, 727-734. Barton, J. K. *Chem. Eng. News* **1988**, *66*, 30-42. Barton, J. K.; Pyle, A. M. *Prog. Inorg. Chem.*, in press. Pyle, A. M.; Long, E. C.; Barton, J. K. *J. Am. Chem. Soc.* **1989**, *111*, 4520. Chow, C. S.; Barton, J. K. *J. Am. Chem. Soc.* **1990**, *112*, 2839.
(2) Bocarsly, J. R.; Barton, J. K. *Inorg. Chem.* **1989**, *28*, 4189-4190. Bocarsly, J. R.; Barton, J. K. Unpublished results.
(3) Anderegg, G. In *Comprehensive Coordination Chemistry*; Wilkinson, G., Ed.; Pergamon Press: New York, 1987; Vol. 2, Chapter 20.3.
(4) Tsuchiya, R.; Uehara, A.; Kyuno, E. *Bull. Chem. Soc. Jpn.* **1971**, *44*, 710-704. Irving, H. M. N. H.; Al-jarrah, R. H. *Anal. Chim. Acta* **1972**, *60*, 345-355.
(5) Abbreviations used: Im, imidazole; NTA, nitrilotriacetate acid; LDA, leucine-*N*,*N*-diacetic acid (*N*,*N*-bis(carboxymethyl)leucine); PDA, phenylalanine-*N*,*N*-diacetic acid (*N*,*N*-bis(carboxymethyl)phenylalanine).

0020-1669/90/1329-4898$02.50/0

spectra were taken by dissolving a finely ground powder in water, followed by rapid filtration and spectroscopy. Chromium concentrations for calculation of ϵ and $\Delta\epsilon$ were then determined by alkaline hydrogen peroxide oxidation to chromate ion,[6] using $\epsilon_{372} = 4815\ M^{-1}\ cm^{-1}$.[7]

^1H NMR spectra were recorded either on a Varian VXR-300 (Bruker magnet) or a VXR-400 system (Oxford magnet). Ligand spectra were taken in D_2O containing 50 mM Na_2CO_3 with sodium 3-(trimethylsilyl)-1-propanesulfonate as standard. The chemical shifts are dependent on solvent and ionic strength. ^2H NMR spectra were taken at 38 MHz on an IBM-Bruker spectrometer or at 61 MHz on a Varian VXR-400 spectrometer. A 5–10 mL aliquot of an approximately 10 mM solution of complex in 10-mm tubes was used for data acquisition. Typically, an acquisition time of ~0.5 s was used. A total of 2000 transients were collected and the free induction decay was processed with 5–10 Hz line broadening. Either an internal standard of C^2HCl_3 in a coaxial tube or an external C^2HCl_3 standard was used, assigning the standard resonance a value of 7.24 ppm.

Aquation Studies. $Cr(NTA)(Im)_2$ was observed to undergo a pH-dependent thermal reaction in aqueous solution. This reaction was studied in phosphate–citrate buffer solutions[8] adjusted to a constant ionic strength of 0.5 M with KCl, at pH 6 and 7 at 25 °C. The initial concentration of complex was generally $\sim 9 \times 10^{-3}$ M; the pH change during reaction (24–27 h) was ~+0.15 pH units. Due to the relative slowness of dissolution of the solid complex even when finely ground (ca. 15–20 min with vigorous agitation), the solutions were prepared by dissolving a finely ground powder in thermally equilibrated buffer and then rapidly filtering the solution into a cuvette. The reaction was followed at 630 nm. The apparent first-order rate constants for each reaction were obtained from least-squares fits of plots of ln $(A - A_i)$ vs time, where A is the instantaneous absorbance and A_i is the absorbance at complete reaction. A_i was taken as the constant value reached after ~5 half-lives. The data proved to give acceptable linear fits out to ~4 half-lives, with correlation coefficients (R^2) for the linear least-squares fits of ~0.98. The structure of the product complex was investigated with ^2H NMR spectroscopy by using the deuterated complex.

Synthesis. All reagent grade solvents and solids were used without further purification, with the exception of imidazole, which was sublimed before use. Chromium(III) acetate was purchased from Alfa and was used as received. Nitrilotriacetate and all amino acids were purchased from Aldrich and were used as received. Preparations of the deuterated complex were performed by using standard Schlenk techniques under an atmosphere of dry nitrogen.

Synthesis of $Cr(NTA)(H_2O)_2$ (1). $Cr(CH_3COO)_3 \cdot H_2O$ (2.47 g, 10.0 mmol) and NTA (1.92 g, 10.0 mmol) were combined in 80 mL of a 1:1 methanol–water (v/v) solution and heated to reflux. The color of the solution began to change from forest green to deep violet after ~30 min of refluxing. Reflux was continued for 150 min. The solution was then evaporated to dryness in vacuo by using a water bath (30 °C) to remove the acetic acid byproduct. The resulting purple residue was recrystallized from a 1:1 or 2:1 mixture of dimethylformamide–water (60 mL). Slow evaporation of this solution afforded a microcrystalline solid, which was then washed with 3 × 20 mL of 9:1 ethanol–water and allowed to air dry. Recrystallization of this complex was not found to be a requirement for the addition of the imidazole ligands and completion of the synthesis of **2**. Elemental analysis showed that the solid contains one molecule of dimethylformamide per two molecules of metal complex. Anal. Calcd for $C_6H_{10}NO_8Cr \cdot {}^1/_2C_3H_7NO$: C, 28.81; H, 4.35; N, 6.72. Found: C, 27.67; H, 4.56; N, 6.43.

Synthesis of $Cr(NTA)(Im)_2$ (2). $Cr(CH_3COO)_3 \cdot H_2O$ (2.47 g, 10.0 mmol) and NTA (1.92 g, 10.0 mmol) were combined in 80 mL of a 1:1 methanol–water (v/v) solution and heated to reflux. The color of the solution began to change from forest green to deep violet after ~30 min of refluxing. Reflux was continued for 150 min. The solution was then evaporated to dryness as above, and the violet $Cr(NTA)(H_2O)_2$ residue was dissolved by swirling in 3 mL of water. Then 80 mL of methanol was added, causing some precipitation. The solution was heated to reflux to dissolve the solid. Imidazole (2.72 g, 40.0 mmol) was then added to the hot solution, and refluxing was continued for 50 min. During this period, the solution became purple in color. After refluxing, the solution was evaporated in vacuo to half-volume and was stored at room temperature. Crystalline product precipitated over the next day. The solid was filtered from solution and washed with 4 × 1.5 mL of chilled water, followed by two small portions of ethanol. Yields ranged from 50% to 65%. Elemental analysis showed the solid to contain three waters of crystallization per molecule of complex. Anal. Calcd for $C_{12}H_{14}N_5O_6Cr \cdot 3H_2O$: C, 33.49; H, 4.68; N, 16.28. Found: C, 33.55; H, 4.62; N, 16.28.

Synthesis of Cr(NTA)(Im-*1,2-d*$_2$) (2a). Deuteration of Imidazole.[9] Imidazole (5.04 g, 74.0 mmol) was placed in a dried flask and degassed by repeated vacuum–nitrogen purges. A 30-mL aliquot of 99.8 atom % D_2O was pipetted into the flask. This solution gave a pH meter reading of 9.5 (pD ~9.9). An aliquot of NaOD was added, giving a meter reading of 10.8 (pD ~11.2). The solution was degassed again and was placed in a thermostated oil bath at 49–55 °C for 23 h under an atmosphere of nitrogen. ^1H NMR spectroscopy of the resulting solution indicated 92% exchange at the C2 position. The solution was evaporated to dryness in vacuo by using an oil bath (50–55 °C) and the solid was sublimed up to 90 °C. After sublimation was complete, the solid was stored under nitrogen. A total of 2.72 g was collected (52% yield).

Synthesis of Deuterated Complex. $Cr(CH_3COO)_3 \cdot H_2O$ (1.24 g, 5.0 mmol) and NTA (0.96 g, 5.0 mmol) were degassed and combined in 40 mL of a 1:1 CH_3OD–D_2O (v/v) solution. The solution was then degassed again and heated to reflux under a nitrogen atmosphere. Reflux was continued for 200 min. The solution was then evaporated to dryness in vacuo by using a water bath. The resulting purple residue was dissolved in a solution of 1.5 mL of D_2O and 39.5 mL of CH_3OD, followed by degassing. Degassed imidazole-*1,2-d*$_2$ (1.24 g, 17.7 mmol) was added to the solution, which was then refluxed for 45 min. After refluxing, the solution was evaporated in vacuo to a few milliliters and was stored at room temperature. Crystalline product precipitated over the next day. The solid was filtered from solution under nitrogen, washed with a few portions of CH_3CH_2OD and allowed to dry. The solid was then stored under nitrogen. Deuteration at the C2 positions of both rings was confirmed by FAB mass spectrometry; deuterons at the N1 position exchange rapidly and are not observed under the conditions of the FAB experiment.

Synthesis of Cr((*S*)- or (*R*)-LDA)(Im)$_2$ (3a,b). Synthesis of the Ligand. The literature procedure[10] for the synthesis of this ligand consistently gave mixtures of the mono- and bisalkylated amine. The procedure was therefore modified as follows. $ClCH_2COOH$ (18.90 g, 0.20 mmol) was dissolved in 40 mL of water and was treated slowly with $NaHCO_3$ (16.81 g, 0.20 mmol). The solution was diluted with 30 mL of water and was stirred until the pH reached ~6.3. (*S*)-Leucine or (*R*)-leucine (13.12 g, 0.10 mol) was dissolved in 50 mL of water containing NaOH (4.00 g, 0.10 mol). The two solutions were combined and heated on a water bath to 80–85 °C. After 20 min of heating, dropwise addition of a solution of NaOH (8.01 g, 0.20 mol) in 30 mL of water was started. This solution was added over 40 min while the temperature was maintained in the range 87–91 °C. Heating was continued for 10 min, at which point dropwise addition of a second solution of $ClCH_2COOH$ (9.45 g, 0.10 mol), neutralized with $NaHCO_3$ (8.40 g, 0.10 mol), in 30 mL of water, was started. This solution was added over 10 min with heating, which was continued for an additional 20 min. The solution was then allowed to cool to room temperature, followed by acidification to pH 2.0 with concentrated HCl (18.4 mL). Within 1 h, a waxy white solid precipitated. The solid was filtered from solution and washed with 5 × 100 mL of chilled water. Purification was achieved by placing the wet solid in 40 mL of water and heating the solution gently until all solid dissolved. The solution was allowed to cool to room temperature and was stored at room temperature overnight to allow the product to precipitate. The solid was then filtered from solution and washed with 5 × 100 mL of chilled water and dried in vacuo. A total of 7.48 g was collected (30% yield).

Synthesis of the Complex. $Cr(CH_3COO)_3 \cdot H_2O$ (2.50 g, 10.1 mmol) and (*S*)- or (*R*)-LDA (2.50 g, 10.1 mmol) were placed in 60 mL of a 2:1 methanol–water (v/v) solution and heated to reflux. Heating was continued for 210 min, and the solution was evaporated to dryness in vacuo. Then 4 mL of water was added, and the solution was swirled gently by hand to dissolve the residue. Vigorous stirring (e.g., by a magnetic stirrer) caused rapid precipitation of solid. After the solid was dissolved, the solution was stored at room temperature overnight to allow crystallization of the product, which precipitated as a microcrystalline solid. The solid was then filtered from solution, washed with 2 × 10 mL of a 3:1 acetone–ethanol (v/v) solution, and allowed to air dry. A total of 0.96 g of product was collected. This material was heated to reflux in 46 mL of a 30:1 methanol–water (v/v) solution. After the solid dissolved, imidazole (0.79 g, 11.6 mmol) was added to the hot solution and reflux was continued for 50 min. The solution was then allowed to evaporate slowly. After 6 days, a microcrystalline solid was filtered from solution and washed with 10 mL of a 1:1 acetone–ethanol (v/v) solution in small

(6) Kirk, A. D.; Namasivayam, C. *Inorg. Chem.* **1988**, *27*, 1095–1099.
(7) Haupt, G. *J. Res. Natl. Bur. Stand. (U.S.A.)* **1952**, *48*, 414.
(8) Elving, P. J.; Markowitz, J. M.; Rosenthal, I. *Anal. Chem.* **1956**, *28*, 1179–1180.
(9) Wong, J. L.; Keck, J. H., Jr. *J. Org. Chem.* **1974**, *39*, 2398–2403.
(10) Uehara, A.; Kyuno, E.; Tsuchiya, R. *Bull. Chem. Soc. Jpn.* **1970**, *43*, 414–418.

portions. A total of 0.19 g was collected. Elemental analysis indicated that the solid contained one imidazole and one water of crystallization per molecule of complex. Anal. Calcd for $C_{16}H_{22}N_5O_6Cr\cdot C_3H_4N_2\cdot H_2O$: C, 44.02; H, 5.44; N, 18.91. Found for **3a**: C, 45.14; H, 5.44; N, 19.10. The product may be recrystallized either by slowly evaporating a methanol solution or by cooling (−20 °C) a methanol solution. In this case, only one water of crystallization is found per molecule of complex. Anal. Calcd for $C_{16}H_{22}N_5O_6Cr\cdot H_2O$: C, 42.67; H, 5.37; N, 15.55. Found: C, 42.81; H, 5.41; N, 15.46.

Synthesis of Cr((*S*)- or (*R*)-PDA)(Im)$_2$ (4a,b). Synthesis of the Ligand. This ligand was synthesized by a modification of a literature procedure,[11] as the published synthesis consistently gave mixtures of the mono and bisalkylated amine. $ClCH_2COOH$ (18.90 g, 0.20 mol) was dissolved in 85 mL of water and was treated slowly with $KHCO_3$ (20.03 g, 0.20 mol). The solution was stirred until the pH reached ~7.5. (*S*)-Phenylalanine or (*R*)-phenylalanine (16.52 g, 0.10 mol) was dissolved in 85 mL of water containing KOH (5.61 g, 0.10 mol). The two solutions were combined and heated on a water bath to 70 °C. After 11 min of heating, dropwise addition of a solution of KOH (11.23 g, 0.20 mol) in 30 mL of water was started. The solution was added over 47 min while the temperature was maintained in the range 88–92 °C. Heating was continued for 13 min at which point dropwise addition of a second solution of $ClCH_2COOH$ (9.45 g, 0.10 mol) neutralized with $KHCO_3$ (10.01 g, 0.10 mol) in 30 mL of water was started. This solution was added over 8 min with heating, which was continued for an additional 22 min. The solution was then allowed to cool to room temperature, after which it was acidified with concentrated HCl (25 mL) to pH 1.5. The solution was stored covered at room temperature overnight to allow precipitation of the product. The solid was then filtered from solution and washed with 4 × 50 mL water. The moist solid was recrystallized from 9:1 acetone–water (v/v) solution (150 mL). Recrystallization was repeated twice from 3:1 and 3:2 acetone–water (v/v) until the product was pure by NMR. A total of 9.13 g was collected (32% yield).

Synthesis of the Complex. $Cr(CH_3COO)_3\cdot H_2O$ (1.76 g, 7.12 mmol) and (*S*)- or (*R*)-PDA (2.00 g, 7.12 mmol) were placed in 60 mL of a 2:1 methanol–water (v/v) solution and heated to reflux. Heating was continued for 210 min, and the solution was then evaporated to dryness in vacuo. The solid residue was then dissolved in 100 mL of a 1:1 methanol–water (v/v) solution and placed in an evaporating dish (50 × 100 mm). After 2 days, the dish was partially covered to slow the evaporation. A microcrystalline solid precipitated during the next day. The solid was filtered from solution and washed with 2 × 10 mL of a 9:1 acetone–water (v/v) solution and allowed to air dry. A total of 0.66 g of product was collected. This material was placed in 31 mL of a 30:1 methanol–water (v/v) solution with imidazole (0.49 g, 7.18 mmol) and heated to reflux for 50 min. The hot solution was allowed to cool to room temperature and was then evaporated in vacuo to ~2 mL volume. A 8-mL aliquot of methanol and 10 mL of toluene were added, and the solution was stored at −20 °C. After 2 days, a crystalline product was filtered from solution; 0.67 g was collected. Elemental analysis indicated that the solid contained half a toluene and one methanol of crystallization per molecule of complex. Anal. Calcd for $C_{19}H_{20}N_5O_6Cr\cdot{}^1/_2C_7H_8\cdot CH_3OH$: C, 51.84; H, 5.18; N, 12.86. Found for **4a**: C, 51.00; H, 5.32; N, 13.15.

X-ray Crystallography. Data was collected for both structures at ambient temperature with a θ–2θ scan mode (**3a**) or Wycoff mode (**4a**) using graphite-monochromated Mo Kα radiation. All calculations were performed with the SIEMENS SHELXTL PLUS[12] package.

Structural Determination of $C_{16}H_{22}N_5O_6Cr\cdot H_2O$ (3a). The microcrystalline product was recrystallized from methanol to form large red block crystals. A crystal (0.30 × 0.50 × 0.75 mm) was selected, mounted, and subjected to an X-ray diffraction study. Data were collected on an automated four-circle Nicolet P3 diffractometer (Washington University). An orthorhombic cell was deduced from centering, indexing, and least-squares fitting of 15 independent reflections in the range of $5° \le 2\theta \le 32°$. A total of 5784 reflections in two octants of data, $(+h,+k,+l)$ and $(-h,-k,-l)$, were collected over the range $3.5° \le 2\theta \le 55°$. 3876 reflections of 4902 unique reflections with $F_o > 6\sigma(F_o)$ were considered observed and were used in the following calculations. An empirical absorption correction based on azimuthal scans was applied.

The structure was solved by direct methods and refined by the full-matrix least-squares method, minimizing $\sum w(\Delta F)^2$. All non-H atoms were refined anisotropically. H atoms were constrained to idealized positions (d_{CH} = 0.96 Å; d_{NH} = 0.90 Å) with a common isotropic U value refined to give 0.066 Å^2. H atoms on water were not located. The absolute configuration was determined by Rogers' η refinement test, where η is a chirality parameter included as a prefactor for all $\Delta f''$ values ($\eta = -0.93$ (7)).[13] The final $R(F_o)$ value was 0.0421 and $R_w(F_o)$ = 0.0627 with $w = [\sigma^2(F_o) + 0.0039(F_o)^2]^{-1}$.

Structural Determination of $C_{19}H_{20}N_5O_6Cr\cdot CH_3OH\cdot{}^1/_2C_7H_8$ (4a). The same techniques employed for **3a** were used for **4a**. A dark purple crystal (0.26 × 0.65 × 0.80 mm) of **4a** was selected from the mother liquor and mounted on a glass fiber for data collection on a Nicolet R3m diffractometer (Columbia University). A fast fixed-rate Wycoff scan (19.53°/min) was used over the range $3.0° \le 2\theta \le 55°$ to avoid crystal decay. Three standard reflections were measured every 50 reflections to monitor crystal and instrumental stability, and no significant variation in intensities was found. Of all 6887 reflections collected in the $(+h,+k,+l)$ octant, 2286 reflections with $F_o > 6\sigma(F_o)$ were used in the final analysis. An empirical absorption correction was applied to the data set.

Space group $P2_12_12_1$ (No. 19) was suggested by systematic absences and photographic evidence. Subsequent convergence of the refinement confirmed the space group assignment. Two crystallographically independent molecules were partially revealed by direct-method output. The remaining atoms in these molecules and the solvent molecules were found in the following difference-Fourier map. Anisotropic refinement of all non-H atoms was not possible due to lack of data. Therefore, only the Cr atoms were refined anisotropically. He atoms were placed in their idealized positions by using the riding model, but were not refined. The absolute configuration of **4a** was not determined; however, the presence of the same enantiomer as in **3a** was confirmed by the similarity of the CD spectra of the two complexes (vide infra). The final $R(F_o)$ value was 0.0846 and $R_w(F_o)$ = 0.0985 with $w = [\sigma^2(F_o) + 0.0010(F_o)^2]^{-1}$. The final difference electron-density map was fairly clean (largest peak, 0.64 e/Å^3).

Results and Discussion

Synthesis. Previous synthetic work with chromium(III)–nitrilotriacetate systems has relied on hydroxy-[10,11,14] or bis(μ-hydroxy)-[15] (as opposed to diaquo-) containing intermediates prior to the addition of the final ligands to the remaining cis coordination sites. The use of hydroxide-containing intermediates is not ideal, however, as it may result in low yields due to the precipitation of the metal ion as insoluble chromium hydroxides[16] or in the formation of undesirable hydroxide-containing complexes. Also, the protonation of bridging hydroxide ligands is sometimes required to form the labile diaquo species for substitution reactions to proceed. As such, a diaquo species would be the preferred synthetic intermediate. It has been reported[15] that the diaquo species of the parent complex, $Cr(NTA)(H_2O)_2$ (**1**), could not be isolated as a solid, and its spectroscopic properties were characterized by protonating the bis(μ-hydroxy) compound, $K_2[Cr(NTA)(OH)]_2\cdot 2H_2O$, using 0.1 M $HClO_4$ as solvent.[15] Contrary to this report, the recrystallized solid intermediate, **1**, used in the synthesis of **2** is characterized here. These diaquo complexes can be readily produced without interference of salt byproducts and the labile aquo ligands cannot directly participate in the formation of metal–hydroxide dimers and oligomers and are therefore more "innocent" than hydroxo ligands.

The ligands for the substituted analogues of **2**, (*R*)- and (*S*)-leucine-*N*,*N*-diacetic acid and (*S*)- and (*R*)-phenylalanine-*N*,*N*-diacetic acid, were synthesized by a standard condensation reaction of the appropriate amino acid with excess chloroacetic acid under basic conditions.[17] The ligands were characterized by mass spectrometry[18] and ^{1}H NMR spectroscopy[19] after pu-

(11) Uehara, A.; Kyuno, E.; Tsuchiya, R. *Bull. Chem. Soc. Jpn.* **1971**, *44*, 1548–1551.
(12) Sheldrick, G. M. *Structure Determination Software Programs*; SIEMENS Analytical X-Ray Instruments, Inc.: Madison, WI, 1989.
(13) Rogers, D. *Acta Crystallogr.* **1981**, *A37*, 734–741.
(14) Uehara, A.; Kyuno, E.; Tsuchiya, R. *Bull. Chem. Soc. Jpn.* **1967**, *40*, 2322–2326.
(15) Koine, N.; Bianchini, R. J.; Legg, J. I. *Inorg. Chem.* **1986**, *25*, 2835–2841.
(16) Stunzi, H.; Spiccia, L.; Rotzinger, F. P.; Marty, W. *Inorg. Chem.* **1989**, *28*, 66–71 and references cited therein.
(17) The amino acids used undergo only very slow racemization under the conditions used. See: Bada, J. L. In *Chemistry and Biochemistry of the Amino Acids*; Barrett, G. C., Ed.; Chapman and Hall: New York, 1985; Chapter 13.
(18) Chemical ionization mass spectrometry using either NH_3 or CH_4 as reagent gas produced parent peaks at $m^+ + H = 248$ (LDA) and $m^+ + H = 282$ (PDA). Decomposition pathways characteristic of amino acids, such as peaks consistent with the loss of H_2O and HCOOH, were also observed.

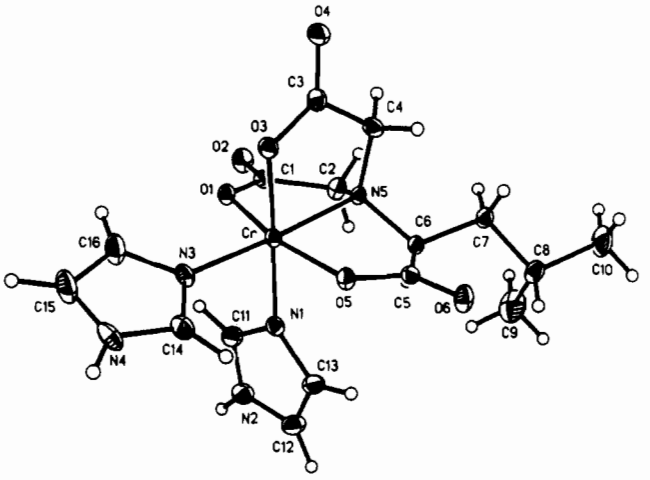

Figure 1. ORTEP representation of **3a** showing 20% probability ellipsoids and atom-numbering scheme. Water of crystallization has been omitted for clarity.

Table I. Crystallographic Data for Complexes $C_{16}H_{22}N_5O_6Cr\cdot H_2O$ (**3a**) and $C_{19}H_{20}N_5O_6Cr\cdot CH_3OH\cdot{}^1/_2C_7H_8$ (**4a**)

	3a	**4a**
empirical formula	$C_{16}H_{22}N_5O_6Cr\cdot H_2O$	$C_{19}H_{20}N_5O_6Cr\cdot CH_3OH\cdot{}^1/_2C_7H_8$
space group	$P2_12_12_1$ (No. 19)	$P2_12_12_1$ (No. 19)
cryst syst	orthorhombic	orthorhombic
unit cell dimens		
a, Å	8.576 (3)	9.601 (4)
b, Å	15.784 (9)	14.045 (4)
c, Å	15.648 (6)	37.235 (11)
V, Å^3	2118 (2)	5021 (3)
Z	4	8
fw	450.4	544.5
T, °C	22	22
diffractometer	Nicolet P3	Nicolet R3m
λ, Å	0.71073 (Mo Kα)	0.71073 (Mo Kα)
ρ_{calcd}, g cm^{-3}	1.412	1.440
abs coeff (μ), cm^{-1}	5.70	4.93
transm coeff	0.799 max/0.611 min	0.437 max/0.385 min
$R(F_o)^a$	0.0421	0.0846
$R_w(F_o)^b$	0.0627[c]	0.0985[d]

[a] $R(F_o) = \sum||F_o| - |F_c||/\sum|F_o|$. [b] $R_w(F_o) = (\sum w||F_o| - |F_c||^2/\sum|F_o|^2)^{1/2}$; $w = [\sigma^2(F_o) + g(F_o)^2]^{-1}$. [c] $g = 0.0039$. [d] $g = 0.0010$.

rification. The metal complexes were then all synthesized by essentially identical routes, with solvent mixtures and methods of crystallization requiring alteration according to the ligand substituent. The complexes were then characterized by standard techniques, including FAB mass spectrometry,[20] visible and infrared spectroscopy,[21] and X-ray crystallography.

X-ray Crystallography. The X-ray diffraction studies of the complexes **3a** and **4a** were undertaken in part to determine the substituent-containing ligand ring in each complex. Each reaction

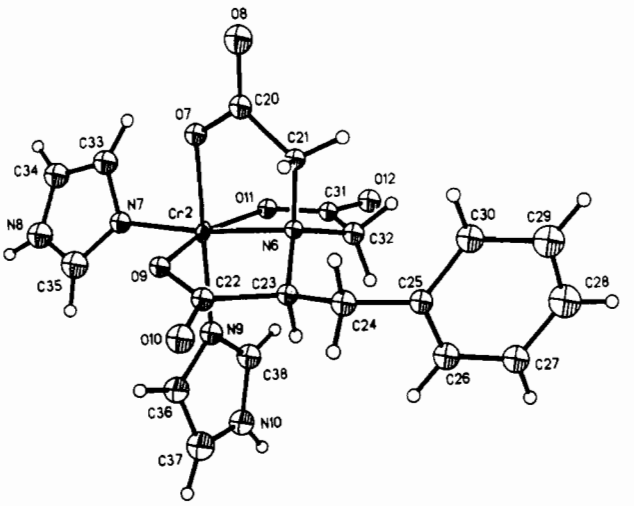

Figure 2. ORTEP representation of molecule 2 of **4a** showing 20% probability ellipsoids and atom-numbering scheme. Solvent molecules of crystallization (CH_3OH, $^1/_2C_7H_8$) omitted for clarity. Atom-numbering scheme for molecule 1 of **4a** correlates to the numbering scheme for molecule 2: $-CH_2-COO$ units, [(O1–C1–O2)–C2 (1), (O7–C20–O8)–C21 (2)], [(O3–C3–O4)–C4 (1), (O9–C22–O10)–C23 (2)], [(O5–C12–O6)–C13 (1), (O11–C31–O12)–C32 (2)]: amine nitrogens, [N1 (1), N6 (2)]; sidechain methylenes, [C5 (1), C24 (2)]; aromatic rings, [C6–C11 (1), C25–C30 (2)]; trans amine imidazole, [N2–C14–C15–N3–C16 (1), N7–C33–C34–N8–C35 (2)]; trans carboxylate imidazole, [N4–C19–C18–N5–C17 (1), N9–C36–C37–N10–C38 (2)].

can produce as many as three isomers, depending on the location of the side chain. Only the initial isomer crystallized was used to complete each synthesis; no attempt was made to purify other isomers. In both cases, this was shown to be the same isomer, with the side chain located on a ring in the equatorial coordination plane. The asymmetric unit cell of **3a** contains one metal complex and one water molecule of crystallization, while the asymmetric cell for **4a** contains two crystallographically independent molecules of complex along with two molecules of methanol and one molecule of toluene. Figures 1 and 2 contain ORTEP representations of the structures of complex **3a** and of one crystallographically independent molecule of **4a** (Figure S1 in the supplementary material contains the second molecule). Table I presents the crystallographic data; Table IIa,b contain atomic coordinates, and selected bond lengths and angles are collected in Table IIIa,b.

There are no literature examples of Cr(III)–nitrilotriacetate systems that have been crystallographically characterized; however, there are a variety of other transition-metal–polyamino polycarboxylate systems that have been structurally characterized for comparison with **3a** and **4a**. The details of the coordination geometry for each complex are typical for polyamino polycarboxylate ligand systems. In an early study of (ethylenediaminetetraacetato)cobalt(III),[22] it was observed that the two coplanar carboxylate-containing five-membered equatorial rings (denoted G, or girdling, rings) exhibited substantially more strain than the out-of-plane rings (termed R, or relaxed, rings). This observation has been borne out in the crystal structures of other polyamino polycarboxylate-containing complexes.[23-26] The same motifs appear in the structures presented in this study. In addition, the G rings of the molecules described here (unlike those in the cobalt–EDTA structure) are inequivalent in that one of the rings contains an amino acid side chain substituent (denoted the G_s ring), while the other is unsubstituted (referred to as G_u). This modification affects the relative degree of strain of the substituted

(19) Couplings were verified by proton-decoupling experiments. Proton designations follow standard amino acid convention, with the exception that the H^α protons on the unsubstituted arms are denoted $H^{\alpha'}$. ^1H NMR for LDA (400 MHz, δ in ppm): 3.83 (AB quartet, 4 H, $H^{\alpha'}$), 3.89 (doublet of doublets, 1 H, H^α), 1.59 (multiplet, 1 H, $H^{\beta 1}$), 1.88 (multiplet, 1 H, $H^{\beta 2}$), 1.81 (multiplet, 1 H, H^γ), 0.94 (doublet, 3 H, $H^{\delta 1}$), 0.98 (doublet, 3 H, $H^{\delta 2}$). Coupling constants (Hz): $J_\alpha - J_{\beta 1} = 5.0$; $J_\alpha - J_{\beta 2} = 8.4$, $J_{\beta 1} - J_{\beta 2} = 13.8$, $J_\gamma - J_{\beta 1} = 8.1$, $J_\gamma - J_{\beta 2} = 5.7$, $J_{\alpha'} - J_{\alpha'} = 16.5$. ^1H NMR of PDA (400 MHz, δ in ppm): 3.78 (AB quartet, 4 H, $H^{\alpha'}$), 4.26 (doublet of doublets, 1 H, H^α), 3.20 (doublet of doublets, 1 H, $H^{\beta 1}$), 3.45 (doublet of doublets, 1 H, $H^{\beta 2}$), 7.39 (multiplet, 5 H, H^{arom}). Coupling constants (Hz): $J_\alpha - J_{\beta 1} = 8.9$; $J_\alpha - J_{\beta 2} = 6.4$; $J_{\beta 1} - J_{\beta 2} = 14.9$; $J_{\alpha'} - J_{\alpha'} = 16.4$.

(20) Characteristic fragments observed include $(m + H)^+ = 377$ (**2**), 379 (**2a**), 433 (**3**), and 467 (**4**), $(m + H)^+ - C_3H_4N_2 - CO_2 = 265$ (**2**), 321 (**3**), and 355 (**4**).

(21) Infrared absorbance was used primarily to verify coordination of the carboxylate ligands to the chromium center and the presence of imidazole. All complexes exhibited both strong asymmetric carboxylate stretches at ~1650 cm^{-1} as well as symmetric stretches around 1380 cm^{-1}. Imidazole ν_{NH} bands appear in the region 2600–3500 cm^{-1}.

(22) Weakleim, H. A.; Hoard, J. L. *J. Am. Chem. Soc.* **1958**, *81*, 549–555.
(23) Swaminathan, K.; Sinha, U. C.; Chatterjee, C.; Yadava, V. S.; Padmanabhan, V. M. *Acta Crystallogr.* **1989**, *C45*, 21–23.
(24) Swaminathan, K.; Sinha, U. C.; Chatterjee, C.; Patel, R. P.; Padmanabhan, V. M. *Acta Crystallogr.* **1988**, *C44*, 447–449.
(25) Gerdom, L. E.; Baenziger, N. A.; Goff, H. M. *Inorg. Chem.* **1981**, *20*, 1606–1609.
(26) Kaizaki, S.; Byakuno, M.; Hayashi, M.; Legg, J. I.; Umakoshi, K.; Ooi, S. *Inorg. Chem.* **1987**, *26*, 2395–2399.

Table II. Atomic Coordinates ($\times 10^4$) and Equivalent Isotropic Displacement Coefficients ($Å^2 \times 10^3$)[a,b]

	x	y	z	U(eq)		x	y	z	U(eq)
				(a) Compound **3a**					
Cr	8335 (1)	2696 (1)	7261 (1)	26 (1)	C4	6322 (5)	3060 (2)	8690 (2)	41 (1)
O1	10077 (3)	2971 (2)	8025 (2)	35 (1)	C5	5536 (4)	1807 (2)	7256 (2)	30 (1)
O2	11082 (3)	2667 (2)	9297 (2)	52 (1)	C6	6214 (4)	1591 (2)	8139 (2)	28 (1)
O3	7428 (3)	3796 (2)	7519 (2)	37 (1)	C7	5013 (4)	1339 (2)	8807 (2)	38 (1)
O4	6077 (3)	4522 (2)	8469 (2)	51 (1)	C8	4414 (5)	428 (2)	8730 (3)	43 (1)
O5	6401 (3)	2268 (2)	6767 (1)	32 (1)	C9	5668 (8)	−211 (3)	8912 (5)	85 (2)
O6	4283 (3)	1513 (2)	7024 (2)	46 (1)	C10	3047 (7)	297 (4)	9315 (4)	76 (2)
N1	9371 (3)	1542 (2)	7026 (2)	33 (1)	C11	10901 (4)	1406 (3)	7123 (3)	43 (1)
N2	11281 (4)	622 (2)	6896 (3)	49 (1)	C12	9945 (5)	227 (3)	6630 (3)	51 (1)
N3	9220 (3)	3168 (2)	6150 (2)	36 (1)	C13	8796 (5)	795 (2)	6699 (3)	45 (1)
N4	9481 (5)	3480 (2)	4804 (2)	53 (1)	C14	8697 (5)	3013 (3)	5369 (2)	49 (1)
N5	7255 (3)	2322 (2)	8382 (2)	28 (1)	C15	10534 (7)	3955 (4)	5226 (3)	68 (2)
C1	10026 (4)	2620 (2)	8769 (2)	34 (1)	C16	10349 (6)	3766 (3)	6070 (3)	60 (2)
C2	8552 (4)	2113 (2)	8974 (2)	38 (1)	O1W	3073 (5)	4252 (2)	9310 (3)	84 (2)
C3	6619 (5)	3865 (2)	8203 (2)	36 (1)					
				(b) Compound **4a**					
Cr1	6012 (4)	4725 (2)	9646 (1)	32 (1)	O12	4813 (14)	3923 (9)	7857 (3)	52 (4)
Cr2	6161 (3)	2087 (2)	7122 (1)	32 (1)	N6	5954 (16)	1526 (9)	7639 (3)	28 (3)
O1	6803 (13)	4667 (8)	10129 (3)	35 (3)	N7	6122 (18)	2606 (10)	6610 (4)	41 (4)
O2	8098 (15)	5479 (9)	10515 (3)	54 (4)	N8	6548 (20)	3190 (13)	6090 (5)	67 (6)
O3	7551 (13)	3960 (8)	9453 (3)	35 (3)	N9	8130 (18)	2630 (12)	7197 (4)	47 (5)
O4	9679 (17)	4046 (10)	9261 (4)	66 (5)	N10	9871 (20)	3543 (14)	7357 (4)	61 (5)
O5	4794 (13)	5762 (8)	9785 (3)	34 (3)	C20	3822 (23)	1046 (13)	7313 (5)	42 (5)
O6	4343 (15)	7275 (10)	9661 (3)	62 (4)	C21	4707 (19)	891 (13)	7639 (5)	34 (5)
N1	7408 (15)	5836 (10)	9563 (3)	31 (4)	C22	7598 (21)	465 (13)	7329 (5)	39 (5)
N2	4758 (19)	3641 (12)	9792 (4)	54 (5)	C23	7263 (20)	993 (13)	7696 (5)	35 (5)
N3	3888 (21)	2475 (13)	10107 (5)	69 (5)	C24	7328 (22)	291 (14)	8021 (4)	47 (5)
N4	5061 (15)	4762 (10)	9146 (3)	32 (4)	C25	7077 (22)	742 (14)	8364 (5)	42 (5)
N5	4630 (19)	4538 (12)	8573 (5)	62 (5)	C26	7961 (25)	1390 (15)	8499 (5)	55 (6)
C1	7615 (19)	5325 (13)	10206 (4)	33 (4)	C27	7810 (24)	1811 (15)	8828 (6)	58 (6)
C2	8098 (21)	5991 (13)	9917 (4)	42 (5)	C28	6617 (27)	1628 (18)	9029 (7)	84 (8)
C3	8566 (24)	4408 (14)	9336 (5)	49 (6)	C29	5636 (27)	990 (17)	8921 (6)	77 (8)
C4	8369 (20)	5498 (12)	9259 (5)	35 (5)	C30	5842 (25)	535 (15)	8562 (5)	56 (6)
C5	9715 (22)	6005 (13)	9208 (5)	49 (6)	C(31)	5265 (20)	3235 (13)	7684 (5)	34 (5)
C6	9551 (21)	7094 (14)	9127 (5)	44 (5)	C(32)	5769 (20)	2356 (12)	7892 (5)	41 (5)
C7	8924 (24)	7378 (14)	8808 (5)	51 (5)	C(33)	4861 (24)	2870 (16)	6440 (6)	58 (6)
C8	8729 (22)	8327 (14)	8730 (5)	51 (6)	C(34)	5210 (26)	3241 (16)	6124 (6)	63 (7)
C9	9112 (25)	9019 (17)	8977 (6)	69 (7)	C(35)	7111 (28)	2776 (17)	6371 (6)	70 (7)
C10	9721 (24)	8722 (16)	9307 (6)	63 (7)	C(36)	9364 (22)	2232 (16)	7096 (5)	57 (6)
C11	9945 (22)	7783 (14)	9371 (5)	50 (6)	C(37)	10434 (27)	2804 (17)	7215 (6)	74 (7)
C12	5122 (21)	6598 (15)	9658 (5)	46 (5)	C(38)	8480 (24)	3450 (17)	7349 (6)	57 (6)
C13	6528 (20)	6658 (14)	9472 (5)	47 (6)	O(1S)	3267 (23)	9798 (15)	1611 (5)	126 (7)
C14	4079 (32)	3011 (20)	9565 (8)	110 (10)	C(1S)	4047 (34)	10650 (20)	1672 (7)	101 (9)
C15	3494 (34)	2297 (24)	9785 (9)	137 (13)	O(2S)	6877 (24)	8933 (15)	9988 (5)	130 (7)
C16	4689 (24)	3230 (15)	10120 (6)	68 (7)	C(2S)	6702 (35)	9836 (24)	9792 (9)	132 (12)
C17	5550 (22)	4351 (13)	8840 (5)	45 (5)	C(39)	8236 (37)	5960 (26)	6573 (10)	119 (12)
C18	3524 (25)	5041 (15)	8700 (6)	64 (7)	C(40)	8240 (44)	6245 (30)	6229 (11)	155 (15)
C19	3817 (23)	5176 (13)	9055 (5)	48 (5)	C(41)	8185 (42)	7128 (33)	6092 (11)	161 (15)
O7	4324 (13)	1547 (8)	7055 (3)	40 (3)	C(42)	8199 (39)	7853 (26)	6351 (10)	138 (13)
O8	2693 (17)	636 (10)	7293 (4)	63 (4)	C(43)	8267 (42)	7607 (28)	6734 (11)	152 (14)
O9	7080 (13)	861 (8)	7053 (3)	34 (3)	C(44)	8355 (37)	6808 (28)	6894 (10)	140 (13)
O10	8387 (15)	−219 (10)	7320 (3)	57 (4)	C(45)	8368 (50)	5061 (34)	6642 (12)	192 (19)
O11	5362 (13)	3226 (8)	7344 (3)	37 (3)					

[a] In this and following tables of crystallographic data, estimated standard deviations in the least significant digit(s) are given in parentheses. [b] Equivalent isotropic U defined as one-third of the trace of the orthogonalized U_{ij} tensor.

ring versus that of the unsubstituted ring, with the presence of the substituent adding a significant amount of ring strain. This difference may be relevant also to the structural understanding of EDTA derivatives incorporated into proteins currently being examined.[27]

Indications of the pattern of ring strain emerge from examination of three structural parameters: the ring torsion angles (O–C–CH_2–N), the angles subtended by the atoms on the mutually perpendicular axes of the octahedron, and the octahedral angles about the Cr centers. In all cases, the observed angles follows the anticipated order of ring strain: $G_s > G_u > R$ (Table IV).

The metal–ligand bond lengths in the two coordination complexes fall within the ranges that are typical for chromium–polyamino polycarboxylate systems. The chromium–amine nitrogen distances, 2.070 (3) (**3a**) and 2.086 (14) Å (**4a**) (average), fall within the typical range of 2.04–2.14 Å.[22-26,28] Likewise, the chromium–oxygen lengths are within characteristic limits of 1.93–1.97 Å. These Cr–O bond lengths do not show obvious correlation with the pattern of ring strain.

The chromium imidazole nitrogen lengths fall into two categories: (a) the imidazole trans to the amine nitrogen and (b) the imidazole trans to the R-ring carboxylate. The trans amine Cr–N_{im} lengths fall in the range 2.015 (17)–2.041 (14) Å, while the trans carboxylate Cr–N_{im} lengths vary from 2.058 (17) to 2.074 (14) Å. The average difference between the two for all structures is 0.03 Å.

Biologically Relevant Solid-State Interactions. The intermolecular interactions within the crystal lattice in the case of both

(27) Rana, J. M.; Meares, C. F. *J. Am. Chem. Soc.* **1990**, *112*, 2457–2458.

(28) Pennington, W. T.; Cordes, A. W.; Kyle, D.; Wilson, E. W., Jr. *Acta Crystallogr.* **1984**, *C40*, 1322–1324.

Table III. Selected Bond Lengths (Å) and Bond Angles (deg)

(a) Compound **3a**			
Bond Lengths			
Cr-O1	1.962 (3)	Cr-O3	1.946 (3)
Cr-O5	1.951 (2)	Cr-N1	2.059 (3)
Cr-N3	2.038 (3)	Cr-N5	2.070 (3)
O1-C1	1.290 (4)	O2-C1	1.228 (4)
O3-C3	1.279 (5)	O4-C3	1.210 (4)
O5-C5	1.291 (4)	O6-C5	1.225 (4)
N5-C2	1.486 (4)	N5-C4	1.493 (5)
N5-C6	1.508 (4)	C1-C2	1.530 (5)
C3-C4	1.505 (5)	C5-C6	1.538 (5)
Bond Angles			
O1-Cr-O3	88.8 (1)	O1-Cr-O5	164.9 (1)
O3-Cr-O5	93.0 (1)	O1-Cr-N1	88.7 (1)
O3-Cr-N1	177.5 (1)	O5-Cr-N1	89.4 (1)
O1-Cr-N3	99.0 (1)	O3-Cr-N3	90.0 (1)
O5-Cr-N3	96.0 (1)	N1-Cr-N3	90.6 (1)
O1-Cr-N5	83.5 (1)	O3-Cr-N5	84.2 (1)
O5-Cr-N5	81.7 (1)	N1-Cr-N5	95.3 (1)
N3-Cr-N5	173.7 (1)		
(b) Compound **4a**			
Bond Lengths			
Cr1-O1	1.955 (11)	Cr1-O3	1.964 (12)
Cr1-O5	1.938 (12)	Cr1-N1	2.080 (14)
Cr1-N2	2.015 (17)	Cr1-N4	2.074 (14)
Cr2-O7	1.936 (12)	Cr2-O9	1.952 (12)
Cr2-O11	1.957 (12)	Cr2-N6	2.091 (12)
Cr2-N7	2.041 (14)	Cr2-N9	2.058 (17)
O1-C1	1.242 (22)	O2-C1	1.258 (21)
O3-C3	1.238 (25)	O4-C3	1.216 (28)
O5-C12	1.303 (23)	O6-C12	1.210 (25)
N1-C2	1.491 (22)	N1-C4	1.537 (22)
N1-C13	1.469 (24)	C1-C2	1.501 (25)
C3-C4	1.570 (26)	C12-C13	1.519 (28)
O7-C20	1.283 (22)	O8-C20	1.229 (26)
O9-C22	1.269 (21)	O10-C22	1.223 (24)
O11-C31	1.270 (21)	O12-C31	1.240 (22)
N6-C21	1.492 (23)	N6-C23	1.478 (24)
N6-C32	1.508 (21)	C20-C21	1.499 (26)
C22-C23	1.586 (25)	C31-C32	1.536 (24)
Bond Angles			
O1-Cr1-O3	91.3 (5)	O1-Cr1-O5	91.2 (5)
O3-Cr1-O5	164.4 (5)	O1-Cr1-N1	85.3 (5)
O3-Cr1-N1	82.6 (5)	O5-Cr1-N1	82.2 (5)
O1-Cr1-N2	87.3 (6)	O3-Cr1-N2	97.8 (6)
O5-Cr1-N2	97.8 (6)	N1-Cr1-N2	172.6 (6)
O1-Cr1-N4	176.6 (6)	O3-Cr1-N4	90.9 (5)
O5-Cr1-N4	87.4 (5)	N1-Cr1-N4	97.6 (5)
N2-Cr1-N4	89.9 (6)	O7-Cr2-O9	92.9 (5)
O7-Cr2-O11	90.9 (5)	O9-Cr2-O11	162.5 (5)
O7-Cr2-N6	83.3 (5)	O9-Cr2-N6	80.3 (5)
O11-Cr2-N6	83.2 (5)	O7-Cr2-N7	90.2 (6)
O9-Cr2-N7	101.6 (5)	O11-Cr2-N7	95.4 (5)
N6-Cr2-N7	173.3 (7)	O7-Cr2-N9	178.7 (6)
O9-Cr2-N9	86.0 (6)	O11-Cr2-N9	90.0 (6)
N6-Cr2-N9	95.9 (6)	N7-Cr2-N9	90.6 (7)

molecules exemplify the biologically relevant interactions that may occur between the complexes and protein surfaces. Two types of interactions are observed in the crystal structures. First, there are apparent hydrogen-bonding interactions in both structures, between coordination complexes and between complexes and solvent molecules. These were isolated by searching for all N–O and O–O nonbonded intramolecular contacts less than 3.1 Å and then examining the available angular relationships to determine the extent to which a linear X–H–Y (X = donor, Y = acceptor) arrangement is found. Table V lists bond lengths and angles for all possible hydrogen bonds. Second, an examination of the crystal data indicates that the weakly polar aromatic–aromatic interactions which have recently been noted[29,30] in protein crystal structures occur between the aromatic rings in the crystal lattice

(29) Singh, J.; Thornton, J. M. *FEBS Lett.* **1985**, *191*, 1–6.
(30) Burley, S. K.; Petsko, G. A. *Science* **1985**, *229*, 23–28.

Table IV. Comparison of Selected Bond Angles (deg) for **3a** and **4a**[a] with Values for the Two Crystallographically Independent Molecules of **4a** Quoted in the Order Molecule 1, Molecule 2

	3a	**4a**
ring torsion angles		
R ring	10.2 (5)	5.9 (2.5), 11.6 (2.2)
G_u ring	−16.7 (4)	−16.5 (2.2), −14.8 (2.3)
G_s ring	30.0 (4)	37.1 (2.1), 25.5 (2.1)
axis bond angles		
$N_{imidazole}$–Cr–O	177.5 (1)	176.6 (6), 178.7 (6)
$N_{imidazole}$–Cr–N_{amine}	173.7 (1)	172.6 (6), 173.3 (7)
O–Cr–O	164.9 (1)	164.4 (5), 162.5 (5)
octahedral angles about Cr		
R: O–Cr–N_{amine}	84.2 (1)	85.3 (5), 83.3 (5)
G_u: O–Cr–N_{amine}	83.5 (1)	82.2 (5), 83.2 (5)
G_s: O–Cr–N_{amine}	81.7 (1)	82.6 (5), 80.3 (5)
$N_{imidazole}$–Cr–$N_{imidazole}$	90.6 (1)	89.9 (6), 90.6 (7)

[a] While some of the differences between the angles in **4a** are not statistically significant, these data generally follow the trend provided both by other structural parameters for **4a** as well as the data for **3a**.

Table V. Bond Lengths and Angles of Apparent Hydrogen-Bonding Interactions in **3a** and **4a**

acceptor–donor (angle used)	dist, Å	angle, deg
Cr((*S*)-LDA)$(Im)_2$ (**3a**)		
O6–N4 (O6–H–N4)	2.867	172
O4–N2 (O4–H–N2)	2.911	154
O4–O_{water} (O_{water}–O4–N2)	2.924	149
O2–O_{water} (O2–O_{water}–O4)	3.029	128
Cr((*S*-PDA)$(Im)_2$ (**4a**)		
O3–N3 (O3–H–N3)	2.899	152
O5–$O_{methanol}$[a] (O5–$O_{methanol}$–$C_{methanol}$)	2.957	97
O8–$O_{methanol}$[a] (O8–$O_{methanol}$–$C_{methanol}$)	2.769	102
O10–N10 (O10–H–N10)	2.696	164

[a] Methanol molecules are crystallographically independent.

of **4a** (involving both complex and solvent).

The crystal lattice of **3a** contains four apparent hydrogen-bonding interactions. All involve the coordinated carboxylate groups of the nitrilotriacetate framework as acceptors. In two of these bonds, the donor groups are imidazole NH protons, and in the other two cases, the donor is a water of crystallization. The bonding relationships are as follows. N4 of one molecule appears to be involved in a bond with O6 of a neighboring complex (2.867 Å). Next, the carbonyl oxygen O4 may be hydrogen bonded both to solvent water and N2 of a neighboring molecule. Finally, the water molecule in turn appears to be bonded to O2 of a neighboring complex in addition to O4. These latter relationships are presented in structure I (Table V). The overall pattern of bonding

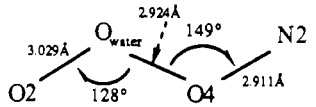

I

in the crystal leads to a hydrogen-bonding network in which all potential bonds on the complex are satisfied.

The hydrogen bonding in the crystal structure of **4a** is similar to that found in **3a**; however, the same number of intermolecular bonds are distributed over the two crystallographically independent molecules of complex. Therefore, not all of the possible hydrogen bonds are satisfied. In addition, while it is the noncoordinated carboxylate oxygens that are the hydrogen bond acceptors in **3a**, in one of the crystallographically independent molecules in the structure of **4a**, it is the coordinated oxygens that serve as the acceptors, a phenomenon that has been observed in similar ligand systems.[23] In the second molecule, the pattern of the noncoordinated carboxylate oxygens serving as acceptors is resumed (Table V).

The possible aromatic–aromatic interactions in **4a** involve the pendant phenylalanine rings of molecules 1 and 2 as well as toluene

Table VI. Geometric Parameters for Aromatic Rings in the Crystal Structure of **4a**[a] (Ring Labeling Scheme: Ring 1 = C6–C11; Ring 2 = C25–C30; Rings T_1 and T_2[b] = C39–C44 (Toluene of Crystallization))

ring	*P* deg	*r*, Å	θ, deg	ϕ, deg	smallest C–C dist, Å
1–2	77.8	5.180	77.7	14.8	C9–C25 (3.859)
2–T_1	61.5	4.895	105.2	170.6	C26–C39b, 3.710
2–T_2	61.5	5.026	102.2	149.8	C29–C40a, 3.780
1–T_1	23.0	6.247			
1–T_2	23.0	9.303			

[a] θ and ϕ values were calculated by projecting the appropriate ring centroid and carbon positions on the mean plane of the required ring. The desired angles were then calculated from these positions. [b] T_1 and T_2 refer to two separate crystallographically identical toluene molecules located in adjacent unit cells, both of which have geometric parameters that fit those for an interaction with ring 2.

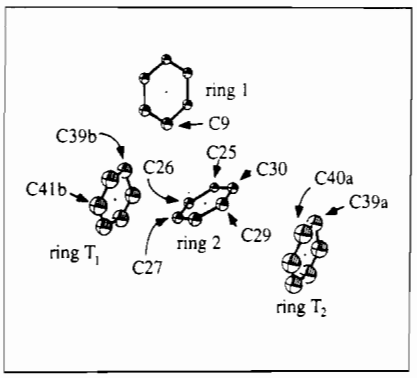

Figure 3. ORTEP representation of the aromatic–aromatic ring interaction in the crystal structure of **4a**. Rings 1 and 2 are the phenylalanine rings of the two crystallographically independent molecules of **4a**. Rings T_1 and T_2 are identical toluene solvent molecules in adjacent unit cells.

solvent molecules of crystallization. Aromatic–aromatic interactions, initially discovered by statistical examination of the relative orientation between aromatic rings in proteins,[29,30] approach a geometry in which the rings are mutually perpendicular, allowing the $\delta(+)$ hydrogens of one ring to interact with the $\delta(-)$ π-electron cloud of the other.[31] The geometric parameters of such edge-to-face interactions have been described by constructing a polar coordinate system that defines the orientation of the donor ring relative to the acceptor ring. The parameters examined (according to Singh and Thornton[29]) are the angle between ring planes (*P*), the position of the donor ring centroid with respect to the acceptor ring centroid in polar coordinates (r, θ, ϕ) (see structure II), and

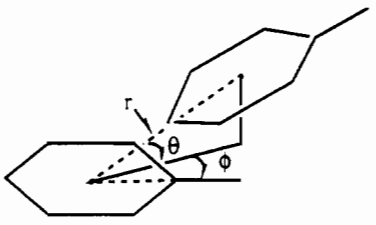

II

the closest carbon–carbon approach between the rings. Typical values from protein-based distributions include a centroid separation of ~5.5 Å[29] (the range is 3.4–5.6 Å) and a mean interplanar angle of 68°.[31] The distribution of closest carbon–carbon lengths has a peak between 3.6 and 4.2 Å.[29] Values for the phenylalanine rings of molecules 1 and 2 and nearby toluene molecules of crystallization appear in Table VI; the geometric relationships between the rings in **4a** is depicted in Figure 3. As can be seen from the values in Table VI, the geometric relationship between rings 1 and 2 (the phenylalanine rings of molecules 1 and 2, respectively) falls well within the distribution of values found for aromatic–aromatic interactions in proteins. The interplanar angle

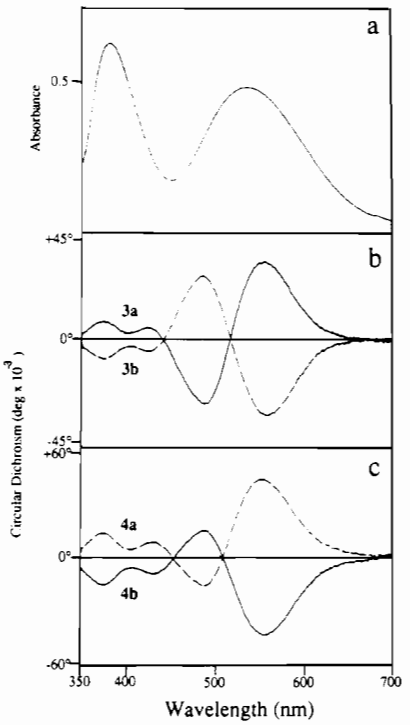

Figure 4. (a) Visible spectrum of **2** (methanol solution, 5 mM). (b) Circular dichroism spectra of **3a,b** (methanol, 5 mM). (c) Circular dichroism spectra of **4a,b** (methanol, 6 mM).

of 77.8° is closer to perpendicular than the mean interplanar angle of 68° found in protein surveys. The centroid separation is slightly lower than the mean protein centroid separation of 5.5 Å. The smallest C–C distance between rings also falls near the center of the distribution found in protein structures. There also appears to be interactions between ring 2 and two nearby toluene molecules of crystallization (rings T_1 and T_2), based on the geometric parameters, such that hydrogens from ring 2 interact with the π-electron clouds of the toluene molecules. The hydrogens involved in these apparent interactions are located on C26 and C29 of ring 2 (Table VI, Figure 3), which are located opposite to each other on the ring, making the dual interaction geometrically possible. Furthermore, there are short carbon–carbon lengths between C27 and C41b (3.883 Å), and C30 and C39a (3.993 Å), suggesting that two protons on each side of ring 2 may interact with the toluene π-electrons. The values for the coordinate ϕ support this possibility, as the observed protein distribution for this parameter has a peak in the 140–150° region, which is proposed to allow a two-hydrogen interaction.[29] As a comparison, the interplanar angle and the centroid separation are included in Table VI for rings 1, T_1, and T_2, which indicate that no interaction occurs between these rings.

The data presented above suggest that there are interlocking aromatic–aromatic interactions between rings 1 and 2 of the two independent complex molecules in the crystal structure of **4a** and with toluene solvent molecules. A hydrogen from ring 1 interacts with the π-cloud of ring 2 and ring 2 hydrogens interact in turn with the toluene π-electrons. These interactions, with the hydrogen bonds discussed above, form a three-dimensional network of interactions within the crystal lattice of **4a**.

Visible and Circular Dichroism Spectroscopy. The complexes have been characterized by visible and circular dichroism spectroscopy (Figure 4). All complexes show two dominant d–d bands. In addition, the visible spectra show very weak features at 674, 700, and 712 nm (not shown), which have been attributed to spin-forbidden transitions and to ligand-to-metal charge-transfer bands, which are thought to be low-energy transitions with small extinctions in the chromium–imidazole system.[32] Finally, the

(31) Burley, S. K.; Petsko, G. A. *J. Am. Chem. Soc.* **1986**, *108*, 7995–8001.

(32) Winter, J. A.; Caruso, D.; Shepherd, R. E. *Inorg. Chem.* **1988**, *27*, 1086–1089.

Table VII. Absorbance and Circular Dichroism Spectra for **2**, **3a,b**, and **4a,b**[a]

complex	band 1		band 2	
	abs λ_{max} (ϵ)	CD λ_{max} ($\Delta\epsilon$)	abs λ_{max} (ϵ)	CD λ_{max} ($\Delta\epsilon$)
$Cr(NTA)(H_2O)_2$ (**1**)[b]	558 (102)		405 (99)	
$Cr(NTA)(Im)_2$ (**2**)	535 (95)		390 (126)	
$Cr(NTA)(Im)_2$ (**2**)[b,c]	535 (111)		389 (137)	
Cr((*S*)-LDA)$(Im)_2$ (**3**)	530 (96)	558 (+0.197)	390 (119)	425 (+0.032)
		488 (−0.163)		375 (+0.049)
Cr((*S*)-PDA)$(Im)_2$ (**4**)	530 (95)	552 (+0.223)	390 (125)	430 (+0.046)
		487 (−0.078)		374 (+0.073)

[a] Spectra were taken in methanol solution, except where indicated. All values are averages based on at least two determinations. Units for λ are nm; units for ϵ and $\Delta\epsilon$ are M^{-1} cm^{-1}. [b] Aqueous solution. [c] Values determined by oxidation of chromium(III) to chromate ion.

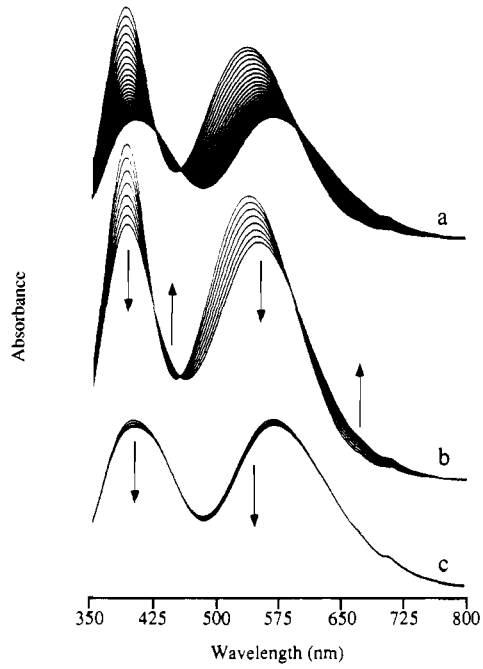

Figure 5. Changes in the visible spectrum of **2** as a function of time at 25 °C in phosphate–citrate buffer at pH 7.01: (a) total change over ~15 h (1 scan/30 min); (b) initial changes over the first hours of reaction (1 scan/30 min); (c) final changes in spectrum after 14 h of reaction (1 scan/60 min). Isosbestic points in part b are located at 426, 456, and 589 nm.

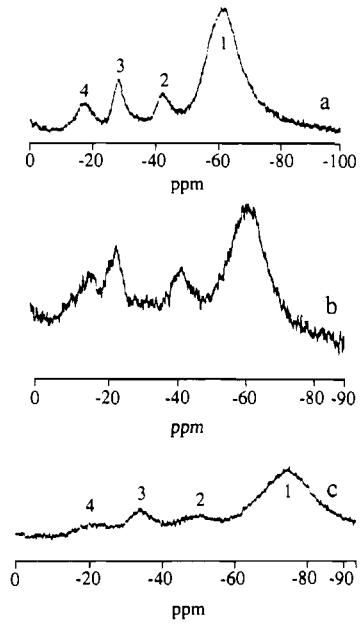

Figure 6. 38-MHz ^2H NMR spectra of **2a** in (a) methanol (ambient temperature); (b) H_2O (ambient temperature); and (c) methanol (−10 °C). Shifts in δ (ppm) in water (w) and methanol (m), based on either an internal or an external C^2HCl_3 standard (7.24 ppm), are as follows: peak 1, −62.2 (w), −60.1 (m); peak 2, −43.2 (w), −42.9 (m); peak 3, −24.4 (w), −28.9 (m); peak 4, −15.9 (w), −18.2 (m).

CD spectra confirm that the absolute configuration of **4a** is the same as the crystallographically determined configuration of **3a**. ϵ and $\Delta\epsilon$ values are listed in Table VII.

Aquation of Cr(NTA)(Im)$_2$ (2). Figure 5a is a typical set of consecutive spectra obtained during reaction of **2** in phosphate–citrate buffer at pH 7.0 (25 °C) over ~15 h. While it appears from Figure 5a that well-behaved isosbestic points are maintained throughout reaction, examination of the changes in the spectrum at long reaction times reveals that this is not so (Figure 5c). Good isosbestic points are, however, observed initially (Figure 5b), suggesting that the reaction is a clean conversion of **2** to product, followed by a secondary reaction of the product. Hence, the reaction appears to be of the form A → B → C. It is apparent from Figure 5c that the spectral change in the 630-nm region at long reaction times is negligible, so the A → B reaction was followed at this wavelength. Plots of ln $(A - A_i)$ versus time (not shown) from which the k_{app} values were calculated both show curvature and are on the border of the acceptable range. The apparent first-order rate constants for the reaction in aqueous solution at 25 °C in phosphate–citrate buffer (0.5 M ionic strength) are 5.9×10^{-5} s^{-1} (pH 6) and 8.0×10^{-5} s^{-1} (pH 7).

The overall reaction involves loss of imidazole ligand, as free imidazole resonances are readily observed in the ^1H NMR spectrum of complex in D_2O. The lability of the chromium–imidazole bond has been previously reported.[32] In order to explicate further the structure of the reaction product, the complex was deuterated at both the 1- and 2-positions of imidazole (**2a**), and the reactant and products were studied by ^2H NMR. Deuterium NMR has been used for structural studies of a variety of deuterated Cr(III) complexes due to the observable NMR line width of deuterium when located on a moiety coordinated to a paramagnetic center such as Cr(III).[33,34] Figure 6 shows spectra of **2a** in methanol and aqueous solution, respectively, taken at ambient temperature. In addition to resonances for HDO and free imidazole-2-*d* (the N(1)–D exchanges rapidly in methanol and water), the spectrum shows four signals. The highest field resonance is appreciably larger in area than the other lower field resonances. A consideration of space-filling models of the complex led to the following interpretation of the spectra. The large high-field resonance (peak 1, Figure 6) is assigned to the imidazole trans to the amine nitrogen, as it can freely rotate around the chromium-nitrogen bond (Figure 7a). In regard to the imidazole ring trans to the carboxylate, three magnetic environments can be postulated: (a) an orientation with the plane of the imidazole parallel to the O–Cr–O axis, with this orientation and the orientation 180° opposite being equivalent (Figure 6, peak 3; Figure 7b); (b) an orientation with the imidazole ring perpendicular to the O–Cr–O axis and with the C2 proton (deuteron) disposed between the nitrilotriacetate methylene protons (Figure 6, peak 2 or 4; Figure 7c or d); (c) a second orientation with the imidazole ring perpendicular to the O–Cr–O axis and with the C4 proton

(33) Johnson, A.; Everett, G. W., Jr. *J. Am. Chem. Soc.* **1972**, *94*, 1419–1425.
(34) Wheeler, W. D.; Kaizaki, S.; Legg, J. I. *Inorg. Chem.* **1982**, *21*, 3250–3252.

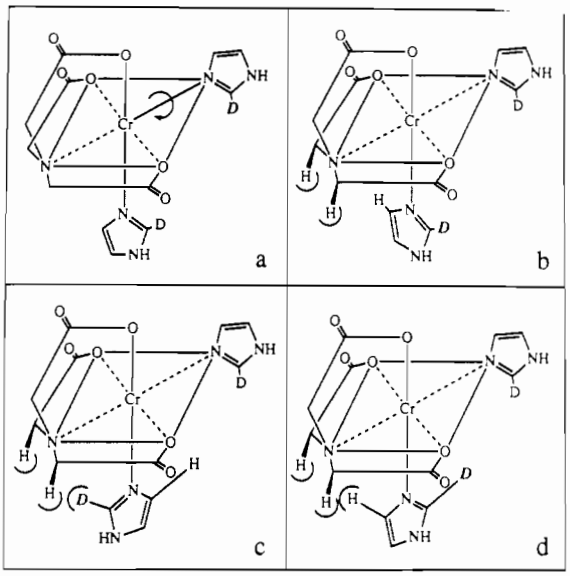

Figure 7. Proposed ^2H magnetic environments for **2a**. The environment depicted in each frame refers exclusively to the deuteron in italic boldface script. Key: (a) trans amine imidazole rotating freely about the Cr–N axis, with the deuteron seeing a single average environment; (b) trans carboxylate imidazole deuteron with imidazole ring parallel to the equatorial O–Cr–O axis; (c) trans carboxylate imidazole deuteron with imidazole ring perpendicular to the equatorial O–Cr–O axis and the deuteron between the nitrilotriacetate methylene protons; (d) trans carboxylate imidazole deuteron with imidazole ring perpendicular to the equatorial O–Cr–O axis and the imidazole C-4 proton between the nitrilotriacetate methylene protons, with the deuteron located roughly under the coordinated nitrogen of the other imidazole ring.

between the methylene protons, i.e., rotated 180° from orientation b (Figure 6, peak 2 or 4; Figure 7c or d).

In an attempt to gain further information about these assignments, the spectrum was measured at −10 °C on the assumption that orientations b and c, which appear to be substantially more sterically hindered than orientation a, would become depopulated at lower temperature. The spectrum obtained is displayed in Figure 6c. While all the peaks broaden at low temperature, the two most intense peaks (peak 1 and peak 3 in Figure 6c) have roughly the same linewidths (measured as full width at half peak height) as they do at ambient temperature (peak 1, 510 (ambient), 550 Hz (−10 °C); peak 3, 190 (ambient), 200 Hz (−10 °C)). Peaks 2 and 4, however, are too broad for any accurate estimation of their line widths, which may indicate that these two peaks are due to depopulated conformational states. The low-temperature spectrum is therefore a further indication that peaks 2 and 4 are appropriately assigned to conformations b and c above Figure 7c and d); peak 3 would then correspond to conformation a (Figure 7b).

Thus the conformation (a) for the trans-carboxylate imidazole ring of $Cr(NTA)(Im)_2$ (Figure 7b) is thought to be the lowest energy orientation for this ring. This accords with the conformation found in the crystal structures of **3a** and **4a** (Figures 1 and 2). In addition, a crude measure of the steric barrier to rotation of the imidazole ring in question about the Cr–N axis is the distance of closest approach of the nitrilotriacetate methylene protons to the C2 and C5 imidazole protons, as determined from the crystal coordinates. In the case of **3a**, this value ranges from approximately 0.9 to 1.3 Å, depending on which combination of protons is considered, suggesting a substantial steric barrier. Given the above assignment scheme, a sample of **2a** was equilibrated in unbuffered H_2O. As can be seen from the initial and final spectra in Figure 8, peak 1 shows an unmistakable decrease in intensity relative to the other peaks in the spectrum, indicating that it is the trans-amine imidazole which leaves in this reaction; presumably its coordination site is filled by an aquo or hydroxo ligand (depending on the pH of reaction).

The conclusions drawn from the ^2H NMR data may be rationalized by considering the ligand set in this complex. Given

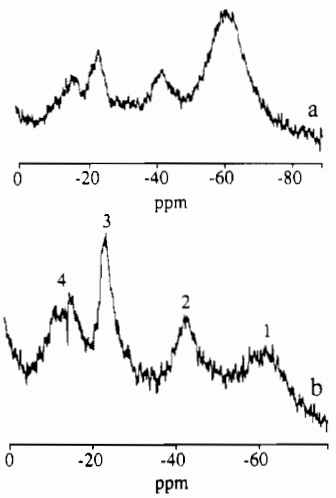

Figure 8. 38-MHz ^2H NMR spectra of **2a** in H_2O: (a) fresh solution; (b) solution after equilibration at room temperature.

Table VIII. Comparison of Carboxylate C–O Bond Lengths (Å) for **3a** and **4a**

	Cr(O—C) length	C=O length	diff
Cr((*S*)-LDA)(Im)$_2$ (**3a**)	1.291 (4)	1.225 (4)	0.066
	1.290 (4)	1.228 (4)	0.062
	1.279 (5)	1.210 (4)	0.069
Cr((*S*)-PDA)(Im)$_2$ (**4a**)[a]	1.238 (25)	1.216 (28)	0.022
	1.303 (23)	1.210 (25)	0.093
	1.242 (22)	1.258 (21)	−0.016[c]
Cr((*S*)-PDA)(Im)$_2$ (**4a**)[b]	1.269 (21)	1.223 (24)	0.046
	1.270 (21)	1.240 (21)	0.030
	1.283 (22)	1.229 (26)	0.054

[a] Molecule 1. [b] Molecule 2. [c] This difference is not statistically significant.

the presence of three carboxylate donors coordinated to the metal center, cis labilization[35] via the carboxylates may play a role. The carboxylate cis labilization effect has previously been observed in group 6 d^6 metal carbonyl complexes[36] of the form $[M(CO)_5(O_2CCX_3)]^-$ (M = Cr, Mo, W; X = H, F). In structurally characterized systems in which cis labilization has been studied,[37,38] this kinetic effect has been associated with an approximate equality in the two C–O bond lengths of the coordinated, cis labilizing carboxylate ligand, despite the fact that one of the two bonds is formally a single bond while the other is formally a C–O double bond. It was observed that in cis-labilizing carboxylate ligands, the difference between the two carboxylate C–O distances averages 0.02 Å, versus a C–O bond length difference of 0.09 Å or greater in systems where cis labilization does not occur.[38,39] The C–O carboxylate bond length differences in the structures of **3a** and **4a** are consistent with this trend (Table VIII). The average C–O difference for the complexes described here (all carboxylates), 0.05 ± 0.03 Å,[40] lies well below the 0.09 Å difference for non-cis-labilizing carboxylates and somewhat above the 0.02 Å value for cis-labilizing carboxylates. This deviation between the difference values found in **3a** and **4a** from those found in the cis-labilizing metal carbonyl complexes may be attributed to the other substantial variations between the two sets of complexes, including differences in the oxidation state of the metal, the charges of the complexes, the bonding characteristics of the ligand set, and

(35) Oldham, C. In *Comprehensive Coordination Chemistry*; Wilkinson, G., Ed.; Pergamon Press: New York, 1987; Vol. 2, Chapter 15.6.
(36) Atwood, J. D.; Brown, T. L. *J. Am. Chem. Soc.* **1976**, *98*, 3160–3166.
(37) Cotton, F. A.; Darensbourg, D. J.; Kolthammer, B. W. S. *J. Am. Chem. Soc.* **1981**, *103*, 398–405.
(38) Cotton, F. A.; Darensbourg, D. J.; Kolthammer, B. W. S.; Kudaroski, R. *Inorg. Chem.* **1982**, *21*, 1656–1662.
(39) Speakman, J. C.; Mills, H. H. *J. Chem. Soc.* **1961**, 1164–1174.
(40) This error is the standard deviation of the differences found in the three crystallographically independent structures of **3a** and **4a**.

Scheme I

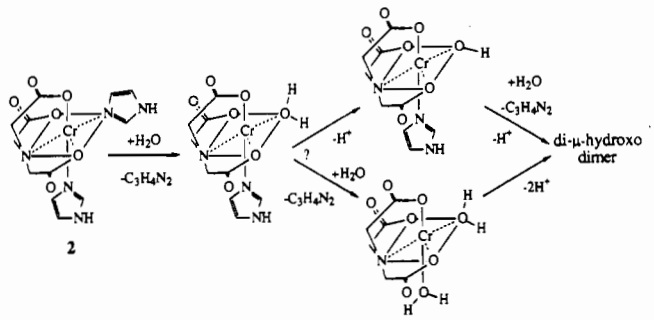

differences in lattice interactions in the solid state (e.g., the metal carbonyl complexes exhibit no evidence of hydrogen bonding in the solid state, while the chromium–nitrilotriacetate complexes do). If the nitrilotriacetate carboxylates are cis labilizing and if the effect is statistical, the trans amine imidazole, which is cis to three carboxylates, is expected to be more strongly labilized than the trans carboxylate imidazole, which has only two cis carboxylates.

In light of this discussion, it should be noted that the trans amine $Cr-N_{imidazole}$ bond lengths in the structures of **3a** and **4a** are shorter than the trans carboxylate lengths, by an average (for all structures) of 0.03 ± 0.02 Å.[40] This may be due to a combination of factors, such as the influence exerted by lattice forces (e.g., hydrogen bonding), which may affect solid-state bond lengths, or it may indicate that these shorter metal–imidazole bonds are more kinetically labile than their longer counterparts.

The changes in the visible spectrum of **2** in aqueous solution are therefore interpreted as follows: Initially, a clean aquation of **2** to Cr(NTA)(Im)(H_2O) involving loss of the trans amine imidazole occurs. As the concentration of Cr(NTA)(Im)(H_2O) builds up, secondary reactions begin, which likely involve the loss of the remaining imidazole and its replacement by an aquo ligand, accompanied by deprotonation of aquo ligand to form a coordinated hydroxide leading to bis(μ-hydroxo) dimer formation. The pK_a of water coordinated to bis(aquo)(nitrilotriacetato)chromium(III), 5.87,[4] and the red shifts in the peaks of the visible spectrum (Figure 5c) support this picture.[15] Scheme I depicts these reactions. At pH values below 6, the initial reaction does not show clean isosbestic points. This may be due to loss of imidazole from both coordination sites; presumably, there is no aquo ligand proton loss at lower pH values. The reaction does appear, however, to proceed much more slowly at lower pH.

Conclusion. We have presented the synthesis, full characterization, and relevant aspects of the solution chemistry of a family of transition-metal complexes that have been designed as inorganic probes of protein structure. Viewed as models for geometry-specific agents for biological targets, these complexes offer the advantages of multiple fixed ligand geometries, a variety of interchangeable biologically relevant ligand sets, and a solution-state lability involving monodentate ligands, which suggests the possibility of covalent interactions with suitable protein side chain moieties. Furthermore, an examination of the solid-state structures of the substituted complexes indicates that both molecules can engage in biologically relevant interactions; in the case where a phenylalanine side chain is used as the substituent, the structural parameters of the aromatic rings in the crystal lattice fit well with those rings observed in protein structures to participate in nonclassical aromatic–aromatic interactions. This illustrates how transition-metal complexes may be constructed with a full array of geometrically fixed weak noncovalent interactions. These interactions, as indicated by our initial studies,[2] can be used to guide metal complex binding with protein surface targets.

Acknowledgment. We are grateful to the NIH (GM33309) for their financial support. We also thank Dr. Kevin Welsh for his help with ^2H NMR experiments and Dr. Christopher Turner for helpful discussions. The Washington University X-ray Crystallography Facility was funded by the NSF Chemical Instrumentation Program (Grant CHE-8811456).

Supplementary Material Available: Full listings of all bond lengths, bond angles, anisotropic displacement coefficients, H atom coordinates, and H atom isotropic displacement coefficients (Tables SIa–SIVa (**3a**) and Tables SIb–SIVb (**4a**)), an ORTEP drawing of molecule 1 of **4a** (Figure S1), and packing diagrams for both structures (Figures S2a (**3a**) and S2b (**4a**)) (10 pages); listings of observed and calculated structure factors (Tables SVa (**3a**) and SVb (**4a**)) (41 pages). Ordering information is given on any current masthead page.